Contrib Mineral Petrol (2012) 164:521–536
DOI 10.1007/s00410-012-0751-7

ORIGINAL PAPER

# Variation of illite/muscovite $^{40}Ar/^{39}Ar$ age spectra during progressive low-grade metamorphism: an example from the US Cordillera

**Charles Verdel · Ben A. van der Pluijm · Nathan Niemi**

Received: 12 December 2011 / Accepted: 7 April 2012 / Published online: 27 April 2012


**Abstract** $^{40}Ar/^{39}Ar$ step-heating data were collected from micron to submicron grain-sizes of correlative illite- and muscovite-rich Cambrian pelitic rocks from the western United States that range in metamorphic grade from the shallow diagenetic zone (zeolite facies) to the epizone (greenschist facies). With increasing metamorphic grade, maximum ages from $^{40}Ar/^{39}Ar$ release spectra decrease, as do total gas ages and retention ages. Previous studies have explained similar results as arising dominantly or entirely from the dissolution of detrital muscovite and precipitation/recrystallization of neo-formed illite. While recognizing the importance of these processes in evaluating our results, we suggest that the inverse correlation between apparent age and metamorphic grade is controlled, primarily, by thermally activated volume diffusion, analogous to the decrease in apparent ages with depth observed for many thermochronometers in borehole experiments. Our results suggest that complete resetting of the illite/muscovite Ar thermochronometer occurs between the high anchizone and epizone, or at roughly 300 °C. This empirical result is in agreement with previous calculations based on muscovite diffusion parameters, which indicate that muscovite grains with radii of 0.05–2 μm should have closure temperatures between 250 and 350 °C. At high anchizone conditions, we observe a reversal in the age/grain-size relationship (the finest grain-size produces the oldest apparent age), which may mark the stage in prograde subgreenschist facies metamorphism of pelitic rocks at which neo-formed illite/muscovite crystallites typically surpass the size of detrital muscovite grains. It is also approximately the stage at which neo-formed illite/muscovite crystallites develop sufficient Ar retentivity to produce geologically meaningful $^{40}Ar/^{39}Ar$ ages. Results from our sampling transect of Cambrian strata establish a framework for interpreting illite/muscovite $^{40}Ar/^{39}Ar$ age spectra at different stages of low-grade metamorphism and also illuminate the transformation of illite to muscovite. At Frenchman Mtn., NV, where the Cambrian Bright Angel Formation is at zeolite facies conditions, illite/muscovite $^{40}Ar/^{39}Ar$ data suggest a detrital muscovite component with an apparent age ≥967 Ma. The correlative Carrara Fm. is at anchizone conditions in the Panamint and Resting Spring Ranges of eastern California, and in these locations, illite/muscovite $^{40}Ar/^{39}Ar$ data suggest an early Permian episode of subgreenschist facies metamorphism. The same type of data from equivalent strata at epizone conditions (greenschist facies) in the footwall of the Bullfrog/Fluorspar Canyon detachment in southern Nevada reveals a period of slow-to-moderate Late Cretaceous cooling.

**Keywords** Geochronology · Thermochronology · Illite/muscovite · $^{40}Ar/^{39}Ar$ dating · US Cordillera

Communicated by T. L. Grove.

**Electronic supplementary material** The online version of this article (doi:10.1007/s00410-012-0751-7) contains supplementary material, which is available to authorized users.

C. Verdel (✉) · B. A. van der Pluijm · N. Niemi
Department of Earth and Environmental Sciences,
University of Michigan, Ann Arbor, MI 48109, USA
e-mail: c.verdel@uq.edu.au

*Present Address:*
C. Verdel
School of Earth Sciences, University of Queensland, Brisbane,
QLD 4072, Australia

## Introduction

K–Ar and $^{40}Ar/^{39}Ar$ step-heating data from micron- to submicron-scale illite/muscovite grains are commonly used to date low-grade metamorphism, deformation, and hydrothermal alteration (e.g., Hunziker et al. 1986; Reuter 1987; Dallmeyer and Takasu 1992; Kirschner et al. 1996; Jaboyedoff and Cosca 1999; Markley et al. 2002; Sherlock et al. 2003; Wyld et al. 2003; Ramírez-Sánchez et al. 2008; Wells et al. 2008; Egawa and Lee 2011; Zwingmann et al. 2011). Most analyses are conducted on aliquots that contain a large number of individual grains, and these mixtures of particularly small grains present challenges for interpretation that are not often encountered in other types of geo- and thermochronology. First, aliquots of clay-sized illite/muscovite from sedimentary rocks typically include both detrital and neo-formed grains (e.g., Hower et al. 1963; Hurley et al. 1963) and therefore include grains that clearly differ in crystallization age and also, potentially, in Ar retentivity. Second, growth of neo-formed illite/muscovite during prograde metamorphism can occur at the expense of pre-existing grains, a process referred to as Ostwald ripening or dissolution/precipitation (e.g., Inoue et al. 1988; Jaboyedoff and Cosca 1999). Third, although Ar diffusion in illite is poorly constrained experimentally, from estimates based on muscovite diffusion parameters (Harrison et al. 2009; Duvall et al. 2011; Rahl et al. 2011), formation of illite/muscovite crystallites during prograde metamorphism may occur first below and subsequently above temperatures at which these crystallites quantitatively retain $^{40}Ar$. Fourth, illite is susceptible to Ar loss both during neutron irradiation (Halliday 1978; Kapusta et al. 1997) and in nature (e.g., Dong et al. 1995; Hall et al. 2000). Finally, as with all thermochronometers, illite/muscovite separates that are sorted by grain-size will produce an age/grain-size correlation arising from differences in diffusion domain size (e.g., Dodson 1973, Harrison et al. 2009).

The cumulative effects of these processes for $^{40}Ar/^{39}Ar$ dating of clay-sized illite/muscovite are complicated step-heating spectra and a correlation between age and grain-size. In many cases, however, this correlation has been attributed solely to simple mixing between detrital and authigenic grains, each with their own distinct "end-member" age (e.g., Pevear 1992; Grathoff and Moore 1996; Clauer et al. 1997; Jaboyedoff and Cosca 1999; Środoń 1999; Grathoff et al. 2001; van der Pluijm et al. 2001). Indeed, controlled $^{40}Ar/^{39}Ar$ experiments on illite and fine-grained muscovite that recognize, or consider, all of the potential complications listed above are rare or nonexistent. To help clarify these issues and test the utility of clay-sized illite/muscovite crystallites as geo- and/or thermochronometers, we collected $^{40}Ar/^{39}Ar$ step-heating data from illite-/muscovite-rich pelitic rocks sampled from a single stratigraphic unit that varies, regionally, in metamorphic grade. Our approach is modeled on a classic study from the Alps (Hunziker et al. 1986) and is analogous to borehole experiments that have been conducted for other thermochronometers (e.g., Gleadow et al. 1986; House et al. 1999; Wolfe and Stockli 2010), with the possible advantage that detrital mineralogy and provenance are expected to vary less within a single, relatively thin stratigraphic datum than in deep boreholes that penetrate multiple formations. Our results are used to infer (1) the temperature range of the illite/muscovite Ar partial retention zone; (2) the relationship between illite crystallite thickness, grain-size, and Ar retentivity; (3) metamorphic conditions leading to dissolution of clay-sized detrital muscovite and Ostwald ripening of neo-formed illite/muscovite; (4) the minimum age of clay-sized detrital muscovite in a sample of Middle Cambrian shale from the Colorado Plateau; (5) the timing of anchizonal metamorphism in the Panamint and Resting Spring Ranges of eastern California; and (6) the Cretaceous cooling rate of the footwall of a Cordilleran metamorphic core complex.

## Considerations for illite/muscovite $^{40}Ar/^{39}Ar$ dating

### Illite to muscovite transition

Illite is a phyllosilicate made up of packets of 1-nm-thick sheets (Fig. 1). Each sheet consists of an octahedral aluminosilicate layer positioned between upper and lower tetrahedral layers, and the sheets themselves are separated by potassium atoms (e.g., Moore and Reynolds 1997). In terms of crystal structure and chemical composition, illite is therefore similar to muscovite. For the purpose of this study, we consider the primary distinctions between illite and muscovite to be grain-size and packet thickness, illite being <2 μm and consisting of packets with comparatively few 1 nm sheets. We use the term "illite/muscovite" when drawing no distinction between the two or when describing particularly thick, micron-scale crystallites, in which case the only practical difference between illite and muscovite is grain-size. When referring to formerly coarse-grained muscovite that has been comminuted to micron scale, we retain "muscovite" for clarity, for example "clay-sized detrital muscovite."

Relative differences in packet thickness of illite/muscovite can be measured with X-ray diffraction (XRD) and are quantified with a parameter called illite crystallinity (IC; e.g., Kübler 1967; Warr and Rice 1994; Kübler and Jaboyedoff 2000). In pelitic rocks, low-grade metamorphic progression from the diagenetic zone to the epizone (roughly equivalent to the transition from zeolite to

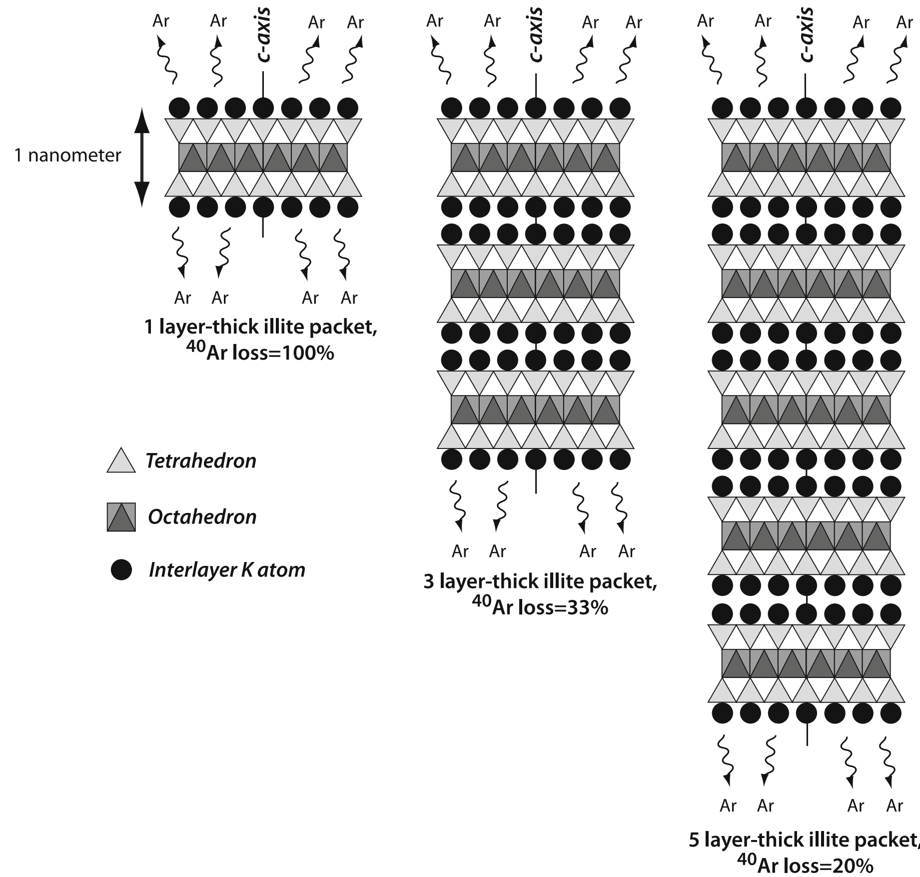


**Fig. 1** Illustration of one-dimensional model for Ar retention in illite/muscovite (Dong et al. 1995)

lower greenschist facies) is marked by a transition from thin illite crystallites to thick illite/muscovite grains that can be tracked with IC (e.g., Hunziker et al. 1986; Weaver 1989; Merriman et al. 1990; Warr and Nieto 1998; Merriman and Peacor 1999). As measured with transmission electron microscopy, the average number of 1-nm sheets per packet can range from <10 for thin illites in diagenetic zone shales to hundreds for thick illite/muscovite in epizonal slates (Merriman et al. 1990). As described below, the thickness of illite/muscovite crystallites has important implications for Ar retention and, by extension, K–Ar and $^{40}$Ar/$^{39}$Ar geochronology.

## $^{40}$Ar loss from low-retention sites in nature

The natural decay of $^{40}$K to $^{40}$Ar releases 28 eV (Dong et al. 1995), corresponding to a $^{40}$Ar recoil distance of ~0.8 nm (calculated using the SRIM 2003 code, http://www.srim.org; Ziegler et al. 1985). Natural "recoil" energy is thus insufficient to eject $^{40}$Ar atoms from interior illite/muscovite interlayers to the packet exterior (a distance $\geq$1 nm in the *c*-axis-parallel direction), but $^{40}$Ar produced from $^{40}$K located on the edges of packets is highly susceptible to loss in nature (Fig. 1; Dong et al. 1995).

Production of $^{39}$Ar from $^{39}$K during neutron irradiation, on the other hand, is significantly more energetic (1–2 × $10^5$ eV; Turner and Cadogan 1974) and has a correspondingly greater recoil distance of ~100 nm. Illite grains typically have thicknesses less than or roughly equal to this distance, so recoil during irradiation is expected to homogenize the $^{39}$Ar distribution in illite/muscovite separates (Dong et al. 1995). A key observation made during step-heating experiments of illite irradiated in vacuum-encapsulated tubes is that the proportion of $^{39}$Ar released before any heating occurs (i.e., the amount that is immediately released when the tube is broken open) is inversely correlated with crystallite thickness (Dong et al. 1995, 1997; Hall et al. 1997, 2000). Based on this finding, it has been inferred that $^{39}$Ar atoms that were recoiled to "unprotected" edges of illite/muscovite packets during irradiation were quickly lost into the encapsulating tube at room temperature and thus that illite edges are non-retentive sites, both for $^{39}$Ar produced during irradiation and for $^{40}$Ar produced in nature. Loss of $^{40}$Ar from the edges of illite packets via this mechanism is analogous to the loss of $^4$He from the edges of apatite and zircon crystals during the much more energetic (4–8 × $10^6$ eV) alpha production from U and Th (e.g., Farley et al. 1996; Reiners 2005).

A one-dimensional model of illite/muscovite Ar retention based on the proportion of K residing on the exterior of packets (Fig. 1; Dong et al. 1995) implies that thin packets have lower Ar retentivity than thick packets, both during laboratory irradiation and in nature. Structural defects in illite/muscovite crystallites are also important pathways for Ar loss (e.g., Hames and Cheney 1997; Kramar et al. 2001; Mulch et al. 2002; Mulch and Cosca 2004; Cosca et al. 2011), and the density of crystallographic defects in illite/muscovite generally decreases as packet thickness increases (e.g., Lee et al. 1985; Jiang et al. 1997; Livi et al. 1997; Warr and Nieto 1998). The contrast in Ar retention between thin and thick crystallites is therefore exacerbated by Ar loss via defects. In this paper, we use "retentive" to describe illite/muscovite crystallites that, by virtue of their relatively large thickness and low defect density, are capable of retaining a large proportion of Ar produced either in nature or during irradiation. According to the one-dimensional retention model, a one-packet-thick illite crystallite is entirely non-retentive because it is predicted to lose 100 % of the $^{40}$Ar produced in nature and $^{39}$Ar produced during irradiation.

Illite "retention ages" were introduced to account for Ar loss from poorly retentive illite (Dong et al. 1995). These are encapsulated $^{40}$Ar/$^{39}$Ar bulk ages that take into account all of the $^{40}$Ar released during step-heating but exclude the $^{39}$Ar that is released when the encapsulating tube is initially broken open. In principle, retention ages from encapsulated aliquots are equivalent to total gas ages produced from non-encapsulated experiments. Encapsulated total gas ages, on the other hand, are equivalent to K–Ar ages (Dong et al. 1995; Onstott et al. 1997). An assumption made during the introduction of retention ages (Dong et al. 1995) that we also make in interpreting our data is that the crystallographic sites in illite/muscovite that are most susceptible to loss of $^{39}$Ar during neutron irradiation are the same sites that are most susceptible to loss of $^{40}$Ar in nature.

## Detrital and neo-formed grains

Siliciclastic rocks, especially pelitic rocks, contain both detrital muscovite and neo-formed illite/muscovite, a factor that introduces complications for geo- and thermochronology, particularly when these grains are mixed together in individual analytical aliquots. In this paper, neo-formed grains are referred to as "authigenic" when they form at particularly low metamorphic grade, as "metamorphic" when they form at approximately greenschist facies, and simply as "neo-formed" for general cases. Shales at very low metamorphic grade (e.g., diagenetic grade, or zeolite facies) contain mixtures of thick, retentive, detrital muscovite grains and thin, less-retentive authigenic illite grains. Separates of illite/muscovite from these low-grade mixtures typically lose significant $^{39}$Ar during irradiation, and $^{40}$Ar/$^{39}$Ar step-heating experiments conducted on them often produce staircase-shaped spectra (e.g., Hunziker et al. 1986; Jaboyedoff and Cosca 1999; Dong et al. 2000; Verdel et al. 2011a). A key point in the interpretation of K–Ar and $^{40}$Ar/$^{39}$Ar data from very low-grade shales is that there is not only a difference in crystallization age between detrital muscovite and authigenic illite but also differences in Ar retentivity between thick muscovite packets (high retentivity, characteristic of detrital muscovite) and thin illite crystallites (low retentivity, characteristic of authigenic illite). At higher metamorphic grade (e.g., anchizone–epizone), four important and related observations have previously been made: average packet thickness is greater (e.g., Merriman et al. 1990; Jiang et al. 1997), crystallographic defects are reduced (e.g., Livi et al. 1997), $^{40}$Ar/$^{39}$Ar spectra are frequently flatter (Hunziker et al. 1986), and there is less $^{39}$Ar loss during irradiation (Dong et al. 1995, 2000). These observations suggest relationships between nanometer-scale crystallographic structure, Ar retention, temperature, and the low-grade metamorphic transition of illite to muscovite.

## $^{40}$Ar loss by volume diffusion

There are currently no experimentally based Ar diffusion parameters for illite, but parameters for muscovite may be good proxies because illite and muscovite are structurally similar (e.g., Parry et al. 2001). Duvall et al. (2011) and Rahl et al. (2011) used muscovite diffusion parameters from Harrison et al. (2009) to calculate theoretical closure temperatures (Dodson 1973) of approximately 250–350 °C for illite/muscovite grains with radii ranging from 0.05 to 2 µm, using cooling rates of 1 to 10 °C/My. Detailed experiments indicate that diffusion of Ar and other elements occurs perpendicular to the c-axis in muscovite (van der Pluijm et al. 1988; Hames and Bowring 1994). Similar experiments are impractical for illite crystallites because of their small size, but we infer that the same diffusion process is true for illite given the structural similarities with muscovite. Cumulatively, these observations suggest that Ar escapes from illite/muscovite in nature primarily via three processes: c-axis perpendicular volume diffusion, loss from low-retention sites on packet exteriors, and loss along microstructural defects. The geometries of grains therefore have important implications for Ar retentivity. Although measurements of the dimensions of individual crystallites is impractical for mixtures containing numerous grains, bulk estimates can be made in the laboratory: grain-size separates based on settling velocity will sort grains primarily by diameter, and thickness variations can be quantified with IC. Diameter and thickness are typically positively correlated (e.g., Hnat 2009), and, as noted earlier, the density of crystallographic defects is inversely correlated with packet thickness.

### Ostwald ripening

Ostwald ripening (Ostwald 1900) refers to the growth of new mineral grains by transfer of material from pre-existing grains. Two common examples of Ostwald ripening are the formation of monazite (e.g., Kingsbury et al. 1993; Ayers et al. 1999; Catlos et al. 2002) and illite/muscovite (e.g., Eberl and Środoń 1988; Inoue et al. 1988; Eberl et al. 1990) during prograde metamorphism. The clearest evidence that Ostwald ripening of illite/muscovite occurs during low-grade metamorphism is a shift to larger particle sizes with increasing metamorphic grade (e.g., Eberl et al. 1988; Jaboyedoff and Cosca 1999; Kim and Peacor 2002). The transfer of $^{40}$Ar during Ostwald ripening and other "illitization" mechanisms is an issue of considerable debate (e.g., Aronson and Hower 1976; Hunziker et al. 1986; Eberl and Środoń 1988; Clauer and Chaudhuri 1996; Velde and Renac 1996; Wilkinson and Haszeldine 2002), but one logical hypothesis is that the process of Ostwald ripening could, under certain conditions, produce large, neo-formed grains with younger ages than the small remnants of older, detrital grains. This relationship would be the opposite of the more frequently encountered positive correlation between age and grain-size that arises from volume diffusion and daughter-isotope recoil/ejection, as described above.

In short, there are competing factors that influence K–Ar and $^{40}$Ar/$^{39}$Ar results from illite separates of siliciclastic rocks, all of which lead to correlations between age and grain-size. Two of the most important considerations are that increased temperature induces both growth of progressively thicker crystallites (e.g., Merriman et al. 1990) and diffusion of $^{40}$Ar out of the crystallites. The first effect increases Ar retentivity, which, in isolation, will lead to older ages. It is countered by the second effect, which produces younger apparent ages. The net result can be evaluated with $^{40}$Ar/$^{39}$Ar step-heating data from samples of illite-/muscovite-rich sedimentary rocks that have experienced a range of metamorphic conditions.

## Field experimental setup

We conducted an experiment utilizing samples collected from a regionally extensive stratigraphic unit in the western United States that has spatial variations in metamorphic grade. This stratigraphic datum consists of Cambrian pelitic rocks that are referred to as the Bright Angel Formation (Fig. 2a) east of the Cordilleran craton–miogeocline hingeline (for example, in locations such as the Grand Canyon) and the Carrara Formation west of the hingeline (for example, in the vicinity of Death Valley). The hingeline separates relatively thin (~1.5 km) Paleozoic stratigraphic sections to the east from much thicker (>6 km) correlative sections to the west (e.g., Wright et al. 1981) and generally corresponds with the leading edge of the Sevier fold-and-thrust belt (Burchfiel and Davis 1972; Burchfiel et al. 1992). The Bright Angel/Carrara Fm. lies near the base of the westward-thickening Paleozoic passive margin sequence and was susceptible to large gradients in metamorphic grade arising from both stratigraphic and tectonic burial (Verdel et al. 2011b).

Samples of Bright Angel/Carrara pelitic rocks were collected along a transect with endpoints at Frenchman Mtn., NV, and Death Valley, CA (Fig. 2a). Clay-mineral characterizations of these samples have previously been reported (Verdel et al. 2011b), and here we focus on the results of encapsulated $^{40}$Ar/$^{39}$Ar step-heating experiments conducted on micron to submicron, illite-/muscovite-rich grain-size fractions of key samples and discuss the implications for illite/muscovite $^{40}$Ar/$^{39}$Ar geo/thermochronology.

## Methods

### Illite crystallinity

Samples were crushed in a mortar and pestle, and <2-μm-grain-size fractions were separated using a centrifuge. This material was mixed with water and pipetted onto glass slides to prepare oriented mounts. These mounts, along with IC standards (Warr and Rice 1994), were scanned from 2 to 50° 2$\theta$ with a Scintag X-1 X-ray powder diffractometer at the University of Michigan. IC was determined from XRD patterns using the MacDiff software program (Petschick et al. 1996).

### $^{40}$Ar/$^{39}$Ar step-heating procedure

Grain-size separates of 0.75–2, 0.2–0.75 μm, and <0.2 μm were prepared with a centrifuge. Approximately 0.1–1 mg of each separate was placed in a quartz glass tube and vacuum-encapsulated prior to irradiation at the McMaster Nuclear Reactor. The MMhb-1 hornblende standard (520.4 Ma; Samson and Alexander 1987) was used as a neutron-fluence monitor. After irradiation, the tubes were broken open under vacuum and step-heated with a continuous argon-ion laser from 0 to 4 W at the University of Michigan. Ar isotopic data were measured on a VG1200S mass spectrometer. Additional details of the analytical procedure are available in Verdel et al. (2011a).

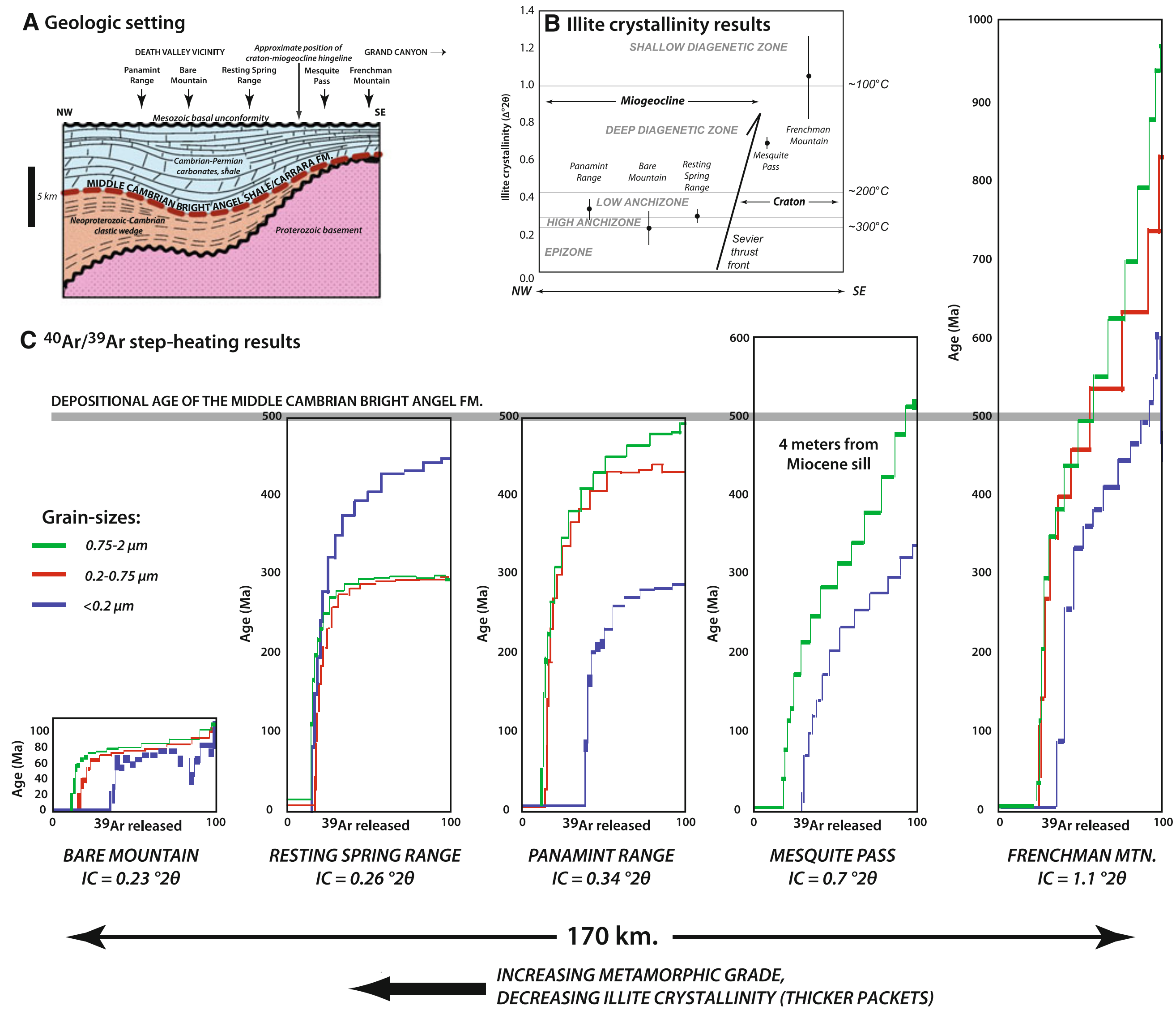


**Fig. 2** Sample positions and experimental results. **a** Highly simplified reconstruction of the Cordilleran miogeocline, after Wright et al. (1981) and Wernicke et al. (1988). Sample positions are shown relative to present-day geographic locations. **b** Illite crystallinity results, after Verdel et al. (2011b). **c** Step-heating results, plotted at equivalent scales. Depositional age of the Bright Angel Fm. from Middleton et al. (2003)

## Results

### Illite crystallinity

Full results of the illite crystallinity study are available in Verdel et al. (2011b), so here we summarize the results that are most pertinent to interpretation of the $^{40}Ar/^{39}Ar$ results. All of the samples have a prominent illite/muscovite diffraction peak at 1 nm, and XRD patterns indicate that illite/muscovite is the predominant K-bearing phase in the <2 µm fraction of each sample (Verdel et al. 2011b). Average IC from two measurements of sample FM09 from Frenchman Mtn., normalized to the standards of Warr and Rice (1994), is 1.1° $2\theta$ (Fig. 2b; Table 1), corresponding with the shallow diagenetic metapelitic zone. Average IC from the Mesquite Pass sample (MP05) is 0.7° $2\theta$, within the deep diagenetic zone. The Panamint Range sample (PR10) has IC of 0.34° $2\theta$ (low anchizone), a slightly greater value than the Resting Spring Range sample (RS03), which has IC of 0.26° $2\theta$ (high anchizone). The average IC of sample 0902 from Bare Mtn. is 0.23° $2\theta$ (epizone), the lowest IC measured during the study. The total range in IC from these five samples is 1.1 to 0.23° $2\theta$, spanning from the shallow diagenetic zone to the epizone

**Table 1** Summary of illite crystallinity and $^{40}Ar/^{39}Ar$ data

| Sample location and number | Geographic coordinates | Illite crystallinity (°2$\theta$, <2 μm) | Grain-size (μm) | Total gas age (Ma) | Retention age (Ma) | Maximum age (Ma) | $^{39}Ar$ loss (%) |
|---|---|---|---|---|---|---|---|
| Frenchman Mountain (*FM09*) | 36.19764N, 115.00635 W | 1.1 | 0.75–2 | 451 | 565 | 967 | 24 |
| | | | 0.2–0.75 | 406 | 515 | 831 | 23 |
| | | | <0.2 | 272 | 394 | 578 | 34 |
| Mesquite Pass (*MP05*) | 35.63154N, 115.60696 W | 0.7 | 0.75–2 | 277 | 329 | 518 | 17 |
| | | | <0.2 | 172 | 233 | 337 | 28 |
| Panamint Range (*PR10*) | 36.58595N, 117.12150 W | 0.34 | 0.75–2 | 367 | 409 | 486 | 12 |
| | | | 0.2–0.75 | 343 | 393 | 442 | 14 |
| | | | <0.2 | 162 | 250 | 285 | 38 |
| Resting Spring Range (*RS03*) | 35.98881N, 116.22201 W | 0.26 | 0.75–2 | 247 | 281 | 297 | 13 |
| | | | 0.2–0.75 | 229 | 272 | 294 | 17 |
| | | | <0.2 | 330 | 380 | 441 | 15 |
| Bare Mountain (*0902*) | 36.83270 N, 116.69244 W | 0.23 | 0.75–2 | 76 | 82 | 108 | 11 |
| | | | 0.2–0.75 | 66 | 78 | 104 | 14 |
| | | | <0.2 | 45 | 68 | 99 | 35 |

and corresponding to estimated peak temperatures of ≤100 °C to ≥300 °C (Fig. 2b; e.g., Merriman and Frey 1999).

### $^{40}Ar/^{39}Ar$ step-heating experiments

$^{40}Ar/^{39}Ar$ step-heating results are in Table S1, illustrated in Fig. 2c and summarized in Table 1. For each sample, we discuss below the maximum age reached during step-heating and the fraction of total $^{39}Ar$ released when the encapsulating tubes were broken open.

#### *Frenchman Mountain*

The 0.75–2 μm grain-size from the Bright Angel Formation at Frenchman Mtn. (FM09) produced a staircase-shaped $^{40}Ar/^{39}Ar$ spectrum that reaches a maximum age of 967 Ma (Table 1). Of the total $^{39}Ar$ in this grain-size, 24 % was released upon breaking open the capsule. The two finer grain-sizes also produced staircase-shaped spectra, but with younger maximum ages (831 and 578 Ma) and with roughly equal or greater $^{39}Ar$ loss during irradiation (23 and 34 %).

#### *Mesquite Pass*

Step-heating data were collected from two grain-sizes of the Mesquite Pass sample (MP05). The larger size (0.75–2 μm) produced a staircase-shaped spectrum with a maximum age of 518 Ma and 17 % $^{39}Ar$ loss during irradiation. The spectrum of the finer size (<0.2 μm) is also staircase-shaped, reaches a maximum age of 337 Ma, and lost 28 % $^{39}Ar$ during irradiation.

#### *Panamint Range*

The coarsest grain-size from the Panamint Range sample (0.75–2 μm) produced a staircase-shaped spectrum reaching a maximum age of 486 Ma and lost 12 % $^{39}Ar$. The 0.2- to 0.75-μm fraction has a maximum age of 442 Ma and lost 14 % $^{39}Ar$. The spectrum from the finest size (<0.2 μm) reaches a maximum age of 285 Ma and lost 38 % $^{39}Ar$.

#### *Resting Spring Range*

For the Resting Spring Range sample, the 0.75–2 μm grain-size has a maximum age of 297 Ma and recoiled 13 % $^{39}Ar$. The 0.2–0.75 μm size has a slightly younger maximum age (294 Ma) and recoiled slightly more $^{39}Ar$ (17 %). Both grain-sizes produced "plateau-like" segments between approximately 280–297 Ma at the highest temperature steps. The finest grain-size (<0.2 μm) produced a much older maximum age of 441 Ma and recoiled 15 % $^{39}Ar$.

#### *Bare Mountain*

Three grain-sizes from Bare Mtn. sample 0902 were analyzed. None produced true plateaus according to most definitions, but they are all characterized by relatively flat spectra in the middle part of the degassing experiment. In the largest size (0.75–2 μm), this middle portion has an age of approximately 80 Ma, and ages are slightly younger in the plateau-like segments of the two smaller sizes. Maximum ages are 99–108 Ma, and $^{39}Ar$ recoil increases from 11 to 35 % with decreasing grain-size.

## Discussion

### General features

$^{40}Ar/^{39}Ar$ step-heating behavior of our samples is highly correlated with both grain-size and IC. There is considerable variation between step-heating results for different grain-size separates from the same sample, suggesting that the separates did not simply sort the broken fragments of an originally uniform population of grains. There was undoubtedly some breaking of grains during crushing, however, which will clearly lead to an overall reduction in the grain-size of the separates compared with in situ grain-size. Nevertheless, the fact that the narrow ranges of grain-size separates produced distinct step-heating results suggests that the separates isolated narrow ranges in the physical dimensions of illite/muscovite crystallites that are at least related to their in situ dimensions, i.e., relatively large in situ grains were concentrated in relatively large grain-size separates.

Maximum ages, total gas ages, and retention ages all become younger as IC decreases (packet thickness increases; Fig. 2c; Table 1). $^{39}Ar$ recoil is correlated with IC increases and grain-size decreases, both of which reflect larger proportions of thin crystallites. With one exception (the Resting Spring Range sample), ages decrease with decreasing grain-size. These general findings are consistent with numerous previous studies (e.g., Perry 1974; Aronson and Hower 1976; Hunziker et al. 1986; Dong et al. 1995, 1997, 2000; Hall et al. 1997, 2000; Jaboyedoff and Cosca 1999; Haines and van der Pluijm 2010).

Our results can be interpreted in terms of the factors discussed above: the influence of detrital grains, loss of Ar from low-retention sites on the edges of illite/muscovite packets, the metamorphic transition from thin to thick crystallites, thermally activated Ar diffusion, and dissolution/Ostwald ripening. Given that our samples are all from the same stratigraphic interval and probably included roughly equivalent detrital muscovite populations, sample-to-sample variation in $^{40}Ar/^{39}Ar$ results primarily reflects the latter four processes.

### Age of detrital muscovite

Our interpretation of the staircase-shaped spectra that characterize $^{40}Ar/^{39}Ar$ results from illite-rich, low-grade shales (e.g., the Frenchman Mtn. sample) is that they reflect mixtures between illite and muscovite crystallites that vary in Ar retentivity. Particularly low-grade shales contain both micron-scale detrital muscovite grains, which tend to be quite Ar-retentive despite their small size, and authigenic illite crystallites, which are characterized by thin packets and low Ar retentivity (Fig. 1; Dong et al. 2000). Initial low-T steps from $^{40}Ar/^{39}Ar$ step-heating of these mixtures extract Ar from the least-retentive grains, which necessarily have the youngest apparent ages. Subsequent higher-T steps degas crystallites with progressively greater retentivity, producing progressively older ages. The highest-T steps extract Ar from the most retentive grains, which, in particularly low-grade samples, are clay-sized detrital muscovite grains. The staircase-shaped spectra are therefore related to a continuum mixture and wide range in Ar retentivity. This explanation is consistent with $^{40}Ar/^{39}Ar$ step-heating results from artificial mixtures of coarse-grained muscovite and diagenetic illite (Onstott et al. 1997). Our interpretation of the old apparent ages often encountered in the high-temperature portions of step-heating spectra of clays is an alternative to the model of Kapusta et al. (1997), which attributes them to $^{39}Ar$ recoil. In contrast to the Kapusta et al. (1997) model, we suggest that the old ages have geologic significance.

When multiple grain-size fractions are prepared from a low-grade shale, the largest and most retentive detrital grains, which will produce the oldest apparent ages, are concentrated in the coarsest fraction. Finer fractions concentrate smaller detrital grains and progressively more of the thin, authigenic, poorly retentive illite crystallites. As a result, maximum age decreases and % $^{39}Ar$ recoiled increases with decreasing grain-size in illite-/muscovite-rich mineral separates from low-grade sediments.

According to this interpretation, the maximum age reached on a step-heating spectrum from a low-grade shale is a minimum estimate for the age of detrital muscovite within the sample. The age is a minimum because any illite/muscovite separation with an upper limit on grain-size (such as those analyzed in this study) is expected to produce a younger maximum age than a hypothetical separation with a slightly coarser upper limit. In theory, at sufficiently coarse size, a plateau-like segment would be produced from high-temperature steps, and this plateau would represent the age of a population of detrital muscovite. In practice, however, this is usually not observed for the grain-sizes typically utilized for illite/muscovite $^{40}Ar/^{39}Ar$ step-heating (Hunziker et al. 1986; Dong et al. 2000; Verdel et al. 2011a).

If the interpretation of step-heating results outlined above is correct, the minimum age of detrital muscovite in the Bright Angel/Carrara stratigraphic datum can be estimated from the maximum age reached during step-heating of the coarsest grain-size separate from the sample that experienced the lowest peak temperature. As determined with IC, this is the Frenchman Mtn. sample. The coarsest grain-size from this sample (0.75–2 μm) reached a maximum step-heating age of 967 Ma (Fig. 2c and Table 1). We suggest that 967 Ma is a reasonable minimum age estimate for detrital, clay-sized muscovite in Cambrian shales of the western United States because K–Ar and $^{40}Ar/^{39}Ar$ ages of ≥1,000 Ma have been determined from coarse-grained muscovite in basement exposures of the Basin and Range (Wasserburg and Lanphere 1965; Reiners et al. 2000), and basement rocks of the western United States were likely the source of detrital minerals, including muscovite, in Cambrian strata of western North America (Gehrels et al. 1995, 2011; Stewart et al. 2001).

## Illite Ar partial retention zone

Only the Frenchman Mtn. sample and the coarsest grain-size from the Mesquite Pass sample have maximum step-heating ages that are older than the depositional age of the Bright Angel Formation, which is ~499 Ma (Fig. 2c; Middleton et al. 2003). This observation, in conjunction with the interpretation of step-heating spectra outlined above, implies that $^{40}Ar/^{39}Ar$ illite/muscovite ages have been partially or entirely thermally reset in the other, higher-grade samples. Maximum ages from the Mesquite Pass sample are 293–449 My younger than equivalent grain-sizes from the Frenchman Mtn. sample, suggesting that the Mesquite Pass sample is, itself, partially reset. Importantly, the Mesquite Pass sample was collected four meters from the edge of a 13-Ma felsic sill (Friedmann et al. 1996). While it is quite possible that elevated temperature in the proximity of the sill partially degassed this sample, $^{40}Ar/^{39}Ar$ spectra of the two Mesquite Pass grain-size fractions reach maximum ages of 518 and 337 Ma, suggesting that detrital muscovite in the shale was not completely reset at 13 Ma.

Temperature sensitivities of various thermochronometers have been estimated empirically using sampling profiles in boreholes and exposed crustal sections (e.g., Gleadow et al. 1986; House et al. 1999; Reiners et al. 2000; Stockli et al. 2000; Wolfe and Stockli 2010). Ages decrease with depth in these studies, often revealing an intermediate depth range in which the retention of daughter nuclides is only partial. We evaluate our data in a similar manner, but in the absence of depth measurements, we substitute IC, a parameter that varies with temperature (Ji and Browne, 2000). By analogy to a plot of age versus depth, we plot maximum ages from $^{40}Ar/^{39}Ar$ spectra vs. IC (Fig. 3). Maximum age is used because it is the apparent age of the most retentive illite/muscovite crystallites in a given grain-size fraction, which, for low-grade samples, correspond with clay-sized detrital muscovite grains. We assume that the detrital muscovite population was equivalent in each of our samples, although the more salient observation is simply that detrital muscovite ages must be older than the depositional ages of the Bright Angel/Carrara Fm., except in cases where those detrital ages have been partially or entirely reset due to heating. Thus, by tracking the decrease in maximum ages with increasing metamorphic grade, we empirically estimate the Ar partial retention zone (PRZ) of clay-sized muscovite.

At Frenchman Mtn., the sample site at lowest metamorphic grade, the maximum age from the coarsest size fraction (0.75–2 μm) is 967 Ma. By analogy with a borehole experiment, the Frenchman Mtn. sample represents the upper, low-temperature part of the borehole. Maximum ages decrease in our samples as IC decreases, in a manner similar to the decrease in age with depth in a borehole. The Resting Spring Range sample has an unusual age–grain-size relationship that is discussed in the following section. Maximum ages from the Resting Spring Range and Panamint Range samples (IC = 0.26 and 0.34° 2$\theta$, respectively) vary from 285 to 486 Ma. These contrast markedly with maximum ages from Bare Mtn. (IC = 0.23° 2$\theta$) of only 99–108 Ma (Fig. 3). There are similar large discrepancies in total gas ages and retention ages for these samples

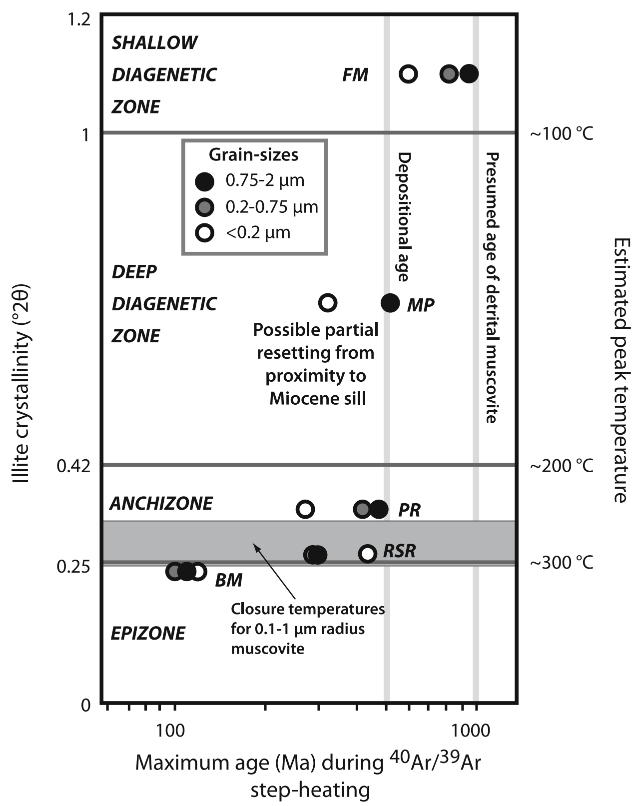


**Fig. 3** "Borehole-like" plot of maximum ages reached on $^{40}Ar/^{39}Ar$ spectra (Fig. 2C and Table 1) versus illite crystallinity, a measure of greenschist to subgreenschist metamorphic grade. Theoretical clay-sized illite/muscovite closure temperature based on muscovite diffusion parameters from Harrison et al. (2009). Presumed age of detrital muscovite is based on ages of ~1,000 Ma from basement exposures in the western United States (e.g., Reiners et al. 2000). See Fig. 2 of Reiners et al. (2000) for an analogous borehole-like muscovite $^{40}Ar/^{39}Ar$ plot from the western United States. *Abbreviations*: *FM* Frenchman Mtn, *MP* Mesquite Pass, *PR* Panamint Range, *RSR* Resting Spring Range, *BM* Bare Mtn

(Table 1). We suggest that this jump to much younger ages, which occurs at metamorphic conditions between those exemplified by the Bare Mtn. and Resting Spring Range samples, represents the base of the illite/muscovite Ar PRZ. This stage of low-grade metamorphism is approximately the anchizone–epizone boundary, which has been empirically calibrated at ~300 °C (e.g., Merriman and Frey 1999). Our empirical estimate for the base of the PRZ is thus consistent with (1) theoretical predictions based on muscovite diffusion parameters, assuming that our nominal grain-size ranges approximate the diffusion length scale (Harrison et al. 2009; Duvall et al. 2011; Rahl et al. 2011); (2) previous comparisons of $^{40}Ar/^{39}Ar$ data from epizonal (Dong et al. 1997) and anchizonal (Dong et al. 1995) pelitic rocks; and (3) general correspondence between illite/muscovite $^{40}Ar/^{39}Ar$ retention ages and zircon fission-track ages (Ramírez-Sánchez et al. 2008). The zircon fission-track partial annealing zone is between about 260° and 310 °C (Tagami and Dumitru 1996), which overlaps with our estimate for the base of the illite/muscovite Ar PRZ.

Our interpretation is that samples from the Resting Spring Range and Panamint Range are within the PRZ. The Mesquite Pass sample is also partially degassed, though presumably from proximity to the Tertiary sill. The pattern of decreasing ages illustrated in Fig. 3 is a direct analog of the finding that muscovite $^{40}Ar/^{39}Ar$ ages decrease with structural depth in an exposed crustal section in the western United States (Reiners et al. 2000). In fact, there is similarity between the overall age ranges obtained in each of these Cordilleran-based empirical thermochronology experiments (compare Fig. 3 with Fig. 2 of Reiners et al. 2000).

## Illite/muscovite dissolution and Ostwald ripening

With one exception, our samples show a relationship between age and grain-size that is typical for thermochronometers, namely younger ages for smaller grain-sizes. The exception is the Resting Spring Range sample, in which the finest grain-size (<0.2 μm) has much older ages, by any measure, than the 0.2–0.75 and 0.75–2 μm fractions (Table 1). The mechanisms described above for Ar retention that we use to evaluate results from the other samples cannot explain this result. We suggest that the combined processes of progressive dissolution of detrital grains and Ostwald ripening of neo-formed crystallites could explain this finding, however. Our interpretation is that for this sample, the finest fraction (<0.2 μm) concentrates the relict cores of detrital muscovite grains, while the coarser fractions concentrate neo-formed illite/muscovite, which, by this stage of metamorphism, have grown to be larger than the remains of the detrital grains (Fig. 4). The finest grain-size separate therefore has the oldest age. As approximated by our IC measurements, this crossing-point in relative crystallite size seems to occur at roughly the transition from low to high anchizone conditions. The transition is superseded at just slightly higher-grade conditions (anchizone–epizone boundary) by complete resetting of $^{40}Ar/^{39}Ar$ ages in micron-scale illite/muscovite.

This overall interpretation is consistent with the finding of Jaboyedoff and Cosca (1999) that grain-sizes of insoluble minerals (including illite/muscovite) increased in a suite of samples during the progression from diagenetic zone to anchizone metamorphism. A subtlety in our interpretation is the inference that detrital muscovite grains are reduced in size during low-grade metamorphism (Fig. 4), a transition that was also noted by Jaboyedoff and Cosca (1999), but which is nevertheless at odds with a continual increase in grain-size arising from Ostwald ripening. Our interpretation is that dissolution of detrital muscovite grains is distinct from Ostwald ripening of neo-formed grains, at least during the earliest stages of metamorphism. This is consistent with the results of detailed laboratory experiments conducted on monazite to stimulate Ostwald ripening under controlled conditions (Ayers et al. 1999). These experiments produced an initial grain-size reduction that was followed by grain-size increase, suggesting an initial phase during which experimental starting minerals (analogous to detrital grains) were partially dissolved, followed by, and possibly overlapping with, an Ostwald ripening phase during which neo-formed grains became larger. An important point is that unless dissolution preferentially removes $^{40}Ar$ over K from detrital grains, partial dissolution, alone, will not directly reduce maximum ages reached on $^{40}Ar/^{39}Ar$ step-heating spectra. Clearly, however, heating of muscovite, either in the laboratory (e.g., McDougall and Harrison 1999) or in nature (e.g., Reiners et al. 2000), will decrease maximum ages via thermal diffusion, independent of the effects of Ostwald ripening.

Given the preceding discussion, similarities in ages between the Resting Spring Range and Panamint Range grain-sizes may be significant. Step-heating results from the <0.2 μm fraction from the Resting Spring Range sample are comparable with results from the 0.75–2 μm and 0.2–0.75 μm fractions from the Panamint Range (Fig. 2c). Likewise, the <0.2 μm Panamint Range fraction has results that are similar to the 0.75–2 and 0.2–0.75 μm Resting Spring Range fractions. These similarities are consistent with the dissolution and Ostwald ripening hypothesis. The 0.75–2 and 0.2–0.75 μm grain-sizes from the Panamint Range sample contain large fractions of partially degassed detrital muscovite and produce maximum step-heating ages of 486 and 442 Ma, respectively (Table 1). Comparable detrital grains, diminished somewhat in size via

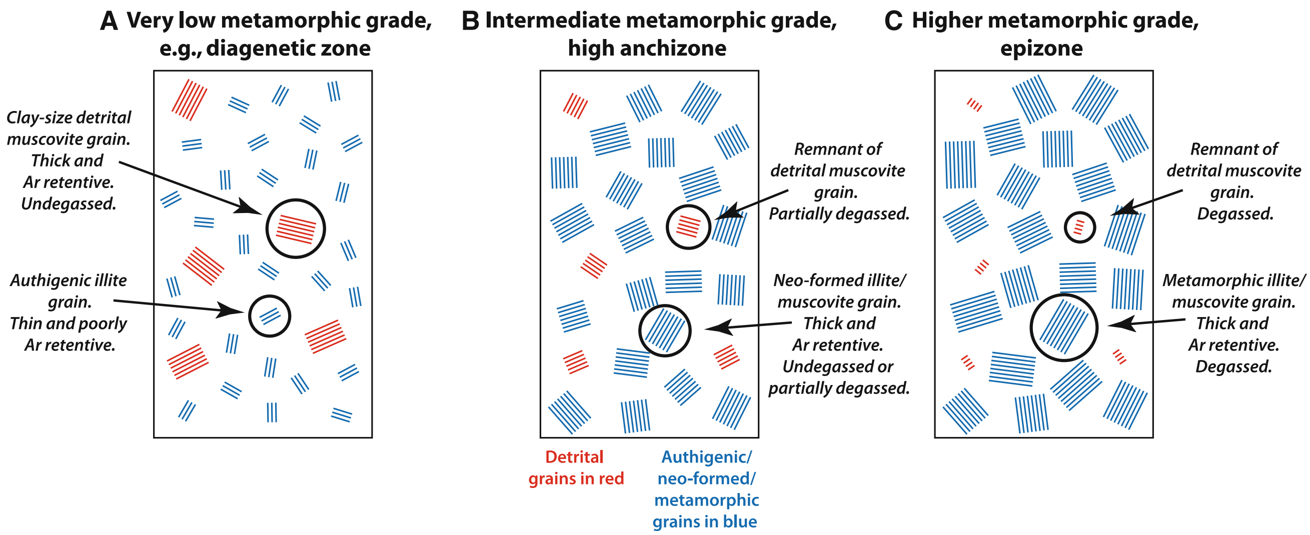


**Fig. 4** Formation of illite/muscovite during low-grade metamorphism. **a** At particularly low metamorphic grade, shales contain mixtures of thick, Ar-retentive, clay-sized detrital muscovite grains and thin, poorly retentive authigenic illite. A wide range of Ar retentivity results in staircase-shaped $^{40}Ar/^{39}Ar$ step-heating spectra. This stage in the formation of metamorphic muscovite is represented by the Frenchman Mtn. sample. **b** With increased temperature, neo-formed illite/muscovite crystallites become thicker and more Ar-retentive. Growth of these grains occurs at the expense of detrital muscovite, so the detrital grains become smaller. At high anchizone conditions, neo-formed illite/muscovite crystallites become larger than the remnants of detrital muscovite, which is a reversal of the size relationship at lower metamorphic grade. Elevated temperature partially degasses both detrital and metamorphic grains at these conditions, though if Ostwald ripening involves reduction in the diameter of detrital grains (as drawn), it would also lower their theoretical closure temperature. The net effect could be that at high anchizone conditions, neo-formed grains have higher closure temperatures than detrital grains. This stage is represented by the Resting Spring Range sample. **c** At epizone conditions, all clay-sized illite/muscovite is fully degassed. K–Ar and $^{40}Ar/^{39}Ar$ results are cooling ages at these and higher-grade conditions. The Bare Mtn. sample is representative of this stage. *Circle diameters* reflect relative crystal size and indicate the formation of large metamorphic muscovite concurrent with a reduction in the size of detrital grains

dissolution, are concentrated in the <0.2-μm fraction of the slightly higher-grade Resting Spring Range sample, which produces a similar (though slightly younger) maximum age of 441 Ma. The <0.2 μm grain-size of the Panamint Range sample, on the other hand, contains a large proportion of relatively small, neo-formed illite/muscovite and produces a younger maximum age of only 285 Ma. The Resting Spring Range counterparts of these neo-formed grains are enhanced in size via Ostwald ripening and therefore concentrated in the larger 0.75–2 μm and 0.2–0.75 μm fractions, but nevertheless produce similar (though slightly older) maximum ages of 297 and 294 Ma, respectively.

In summary, the metamorphic transition from the lower-grade Panamint Range sample to the slightly higher-grade Resting Spring Range sample involves four changes to the step-heating results and their interpretation. First, detrital grains are concentrated principally in coarse grain-size separations at lower metamorphic grade, but in finer size fractions at higher grade. Second, apparent age of the detrital grains decreases with increasing metamorphic grade. Third, there is a parallel increase in the apparent age of neo-formed grains. The cumulative effect is a slight narrowing of the gap in apparent age between detrital muscovite and neo-formed illite/muscovite, consistent with concurrent degassing of the former and increasing Ar retentivity of the latter. A subtle but important consequence of the dissolution/Ostwald ripening process is that decreased crystallite diameter of detrital grains lowers their theoretical closure temperature (Fig. 4), while increased diameter of neo-formed grains has the opposite effect. Therefore, at anchizone conditions partially degassed detrital grains may coexist with undegassed neo-formed grains (Fig. 4). Fourth, step-heating spectra of the grain-size separations that principally concentrate neo-formed grains become flatter with increasing metamorphic grade (compare the spectrum of the <0.2-μm fraction of the Panamint Range sample with spectra from the 0.75–2 and 0.2–0.75 μm grain-sizes in the Resting Spring Range sample), an effect that reflects a narrowing of the range of Ar retentivities in a mixture of crystallites.

The Resting Spring Range sample lies near the base of the illite/muscovite Ar PRZ, so some, or all, of the grain-sizes from it may be partially degassed, in which case their ages may be geologically meaningless, as seems to clearly be the case for the Mesquite Pass grain-sizes. Given the preceding discussion, however, and the form of step-heating results for the 0.75–2 and 0.2–0.75 μm grain-sizes of the Resting Spring Range sample (Fig. 2c), these particular separates seem to contain retentive neo-formed illite/muscovite that could, in fact, preserve meaningful $^{40}Ar/^{39}Ar$ ages. The highest-temperature steps have plateau-like segments that range in age from about 280 to 297 Ma for the 0.75–2 µm grain-size and 280–294 for the 0.2- to 0.75-µm fraction. The final temperature steps from the <0.2 µm fraction of the Panamint Range have comparable ages of 269–285 Ma. These ages may represent prograde muscovite formation in the Resting Spring Range and Panamint Range during early Permian tectonic burial associated with the Sierra Nevada–Death Valley thrust system (SNDVTS; Stone and Stevens 1988; Snow 1992; Stevens and Stone 2005a, b; and see Fig. 4 in Verdel et al. 2011b). The absence of similar ages from the Mesquite Pass and Frenchman Mountain samples suggests that these locations, which are in the foreland of the SNDVTS, were less affected by early Permian tectonism. As discussed below, any indication of early Permian metamorphism has been erased from illite/muscovite $^{40}Ar/^{39}Ar$ results by subsequent heating at Bare Mountain, the highest-grade location we studied.

At epizone conditions, there is a return to the normal relationship of older ages for larger grain-sizes, but with significant differences in $^{40}Ar/^{39}Ar$ step-heating results compared with low-grade samples (Fig. 2c). At epizone conditions and above, metamorphic illite/muscovite crystallites are larger than, and have retentivities at least as great as, detrital muscovite grains (Fig. 4). Relatively flat spectra reflect a comparatively narrow range in Ar retentivity in mixtures within analytical aliquots. Illite/muscovite grains are also degassed at epizone conditions, so we interpret the Bare Mtn. ages as cooling ages. Next, we describe how these data can be used to infer thermal histories.

## Cretaceous cooling at Bare Mountain, NV

Proterozoic to Paleozoic sedimentary rocks were exhumed in the lower plate of the Bullfrog/Fluorspar Canyon detachment at Bare Mountain, NV (Fig. 5; Hoisch et al. 1997; Hoisch 2000). A high-angle normal fault (the Gold Ace fault) within the lower plate of the detachment separates strata metamorphosed up to amphibolite facies in its footwall from greenschist to subgreenschist facies sediments in the hanging wall (Hoisch 2000). Previous muscovite K–Ar and $^{40}Ar/^{39}Ar$ ages from the lower plate of the Bullfrog/Fluorspar Canyon detachment are in the footwall of the Gold Ace fault and range from Miocene to Paleocene (Hoisch et al. 1997). To our knowledge, our illite/muscovite $^{40}Ar/^{39}Ar$ data from the Carrara Fm. are the first thermochronology data from the hanging wall of the Gold Ace fault. Muscovite grains large enough to recognize with a petrographic microscope were not

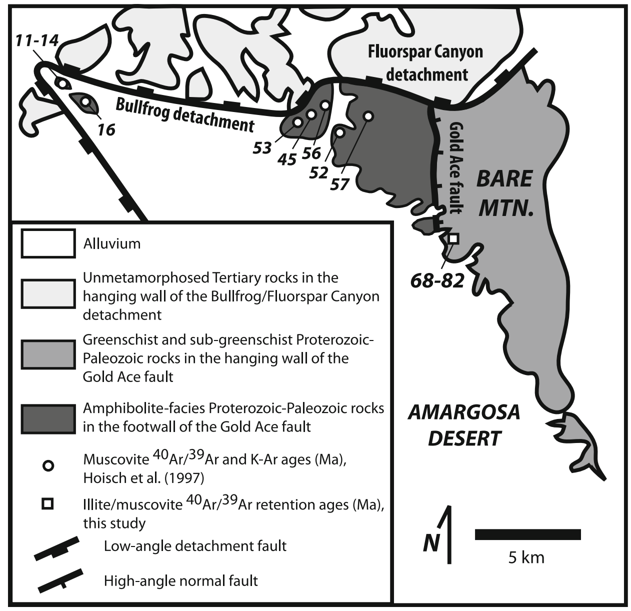


**Fig. 5** Simplified geologic map of Bare Mountain and vicinity (after Hoisch et al. 1997) showing previous muscovite and new illite/muscovite results

observed in our sample, and in general, low metamorphic grade within the hanging wall of the Gold Ace fault may have precluded previous muscovite $^{40}Ar/^{39}Ar$ thermochronology. As in other locations, however, the Carrara Fm. in the hanging wall of the Gold Ace fault is rich in illite/muscovite. Retention ages from three grain-sizes of a sample of the Carrara Fm. are 81.8 ± 0.4, 77.6 ± 0.5, and 67.6 ± 1.6 Ma for grain-sizes of 0.75–2, 0.2–0.75, and <0.2 µm, respectively. Based on the low IC value of this sample, our interpretation is that it was at sufficiently high temperature to completely diffuse $^{40}Ar$ from illite/muscovite, or at least from all but the most retentive grains. The age/grain-size correlation in this case therefore arises from progressive cooling below temperatures at which $^{40}Ar$ is retained in each grain-size.

To estimate a cooling rate for the Bare Mtn. sample, we utilize retention ages and closure temperatures, both of which are simplifications as elaborated below, but nevertheless illustrate a point about the apparent sensitivity of the grain-size separates to different temperatures. Based on diffusion parameters for muscovite (Harrison et al. 2009), closure temperatures for the grain-sizes analyzed are approximately 290, 272, and 249 °C (for domain diameters of 2, 0.75, and 0.2 µm, respectively, cooling rate of 5 °C/My, and spherical diffusion geometry). Using the retention ages as our best estimate of the bulk cooling age for each grain-size, these results indicate a Late Cretaceous period of cooling of the hanging wall of the Gold Ace fault below ~250–290 °C. Furthermore, cooling rate appears to have decreased from about 5 °C/My from approximately

82–78 Ma to ~0.8 °C/My from about 78–68 Ma. Using age differences from just the medium- and high-temperature steps of each grain-size produces similar cooling rate estimates. Our illite/muscovite $^{40}Ar/^{39}Ar$ ages thus overlap with geo- and thermochronology results from the kinematically linked Funeral Mtns. to the SW (Applegate et al. 1992; Beyene 2011) but suggest cooling rates that are slow when compared with Late Cretaceous rates from elsewhere in the Cordilleran orogen (Wells and Hoisch 2008; Chapman et al. 2012).

The use of retention ages and theoretical closure temperatures in the preceding cooling rate estimate might be an inferior approach to modeling continuous thermal histories using Ar release data (e.g., Harrison et al. 2005), particularly given that muscovite appears to be characterized by multiple diffusion domains (Harrison et al. 2009). However, our mineral separates nominally have extremely narrow ranges in grain-size (≤1 μm), so it is not clear that a particular size fraction includes significant variation in domain size. On the contrary, each size fraction may isolate a particular diffusion domain size, in which case the systematic variation in ages from these grain-sizes place an upper limit (200 nm) on the minimum size of muscovite diffusion domains. A mineral separate with a wider range of grain-sizes (and presumably a wider range of domain sizes) may be conducive to thermal modeling and could, in fact, contain the same age–temperature information as multiple grain-size separates. It is important to note, however, that the highest temperature steps from the Bare Mtn. grain-sizes may represent detrital and/or particularly retentive metamorphic illite/muscovite grains that have not been entirely reset, in which case those particular steps are not suitable for continuous thermal modeling. These uncertainties point out the need for additional tests of illite/muscovite $^{40}Ar/^{39}Ar$ thermochronology, but data from Bare Mtn., as well as the other sample sites, illustrate that illite/muscovite grain-size separates that differ in diameter by ≤1 μm preserve distinct age information.

## Conclusions

$^{40}Ar/^{39}Ar$ step-heating results from illite/muscovite in greenschist to subgreenschist pelitic rocks are closely tied to thermal histories. At very low metamorphic grade (e.g., zeolite facies), spectra are typically staircase-shaped, reflecting a mixture between relatively large (but still clay-sized), high-retentivity detrital muscovite grains and smaller, less-retentive authigenic illite grains. Maximum temperature steps from these samples place minimum constraints on the apparent age of detrital muscovite. In the case of the Middle Cambrian Bright Angel Formation at Frenchman Mtn., NV, this minimum age is 967 Ma, consistent with ≥1,000 Ma ages that have been determined from muscovite in basement rocks of the US Cordillera.

As metamorphic grade increases, neo-formed illite/muscovite crystallites become thicker and more Ar-retentive. At approximately the transition from low to high anchizone conditions, retentivity of neo-formed illite/muscovite appears sufficient to produce geologically meaningful ages and plateau-like $^{40}Ar/^{39}Ar$ step-heating spectra. In the Resting Spring Range and Panamint Range of eastern California, the Cambrian Carrara Fm. is at approximately this stage of low-grade metamorphism and contains illite/muscovite that seems to record early Permian metamorphism associated with the Sierra Nevada–Death Valley thrust system.

At greenschist (epizone) conditions, metamorphic illite/muscovite is completely degassed and difficult to distinguish from coarse-grained muscovite in terms of XRD characteristics, although individual grains may still be too small to observe with a petrographic microscope. Under such conditions, illite/muscovite is useful for $^{40}Ar/^{39}Ar$ thermochronology. An example of illite/muscovite $^{40}Ar/^{39}Ar$ thermochronology from the epizonal Carrara Fm. at Bare Mtn., NV, reveals a Late Cretaceous period of cooling at rates of ~1–5 °C/My in the hanging wall of the Gold Ace fault.

Illite/muscovite separates that differ in size by ≤1 μm have distinct $^{40}Ar/^{39}Ar$ step-heating spectra and can vary in apparent age by hundreds of millions of years. These observations suggest that the separates isolate narrow ranges in diffusion domain size, implying that illite/muscovite is characterized by multiple diffusion domains with dimensions of order hundreds of nanometers, if not smaller. Although significant additional work is needed to reliably interpret complex $^{40}Ar/^{39}Ar$ step-heating results from fine-grained illite/muscovite in low-grade sediments, this type of data appears to offer, in combination with illite crystallinity, a geo-thermochronometer/peak-temperature thermometer for low-grade metamorphism.

**Acknowledgments** We thank Chris Hall at the UM Argon Geochronology Laboratory for conducting the $^{40}Ar/^{39}Ar$ step-heating experiments. XRD analysis was conducted in the UM Electron Microbeam Analysis Laboratory. The paper benefited from discussions with Daniel Stockli and comments from Michael Cosca and an anonymous reviewer. This research was supported by NSF grant EAR 0738435 and post-doctoral funds from the University of Michigan.

## References

Applegate JDR, Walker JD, Hodges KV (1992) Late Cretaceous extensional unroofing in the Funeral Mountains metamorphic core complex, California. Geology 20:519–522

Aronson JL, Hower J (1976) Mechanism of burial metamorphism of argillaceous sediment: 2. Radiogenic argon evidence. Geol Soc Am Bull 87:738–744

Ayers JC, Miller C, Gorisch B, Milleman J (1999) Textural development of monazite during high-grade metamorphism: hydrothermal growth kinetics, with implications for U, Th-Pb geochronology. Am Mineral 84:1766–1780

Beyene MA (2011) Mesozoic burial, mesozoic and cenozoic exhumation of the Funeral Mountains core complex, Death Valley, southern California (PhD thesis), University of Nevada, Las Vegas, p 349

Burchfiel BC, Davis GA (1972) Structural framework and evolution of the southern part of the Cordilleran Orogen, western United States. Am J Sci 272:97–118

Burchfiel BC, Cowan DS, Davis GA (1992) Tectonic overview of the Cordilleran orogen in the western U. S. In: Burchfiel BC, Lipman PW, Zoback ML (eds), The Cordilleran Orogen: Conterminous U. S.: The Geology of North America, Vol G-3, Decade of North American Geology, Geological Society of America, Boulder, pp 407–480

Catlos EJ, Gilley LD, Harrison TM (2002) Interpretation of monazite ages obtained via in situ analysis. Chem Geol 188:193–215

Chapman AD, Saleeby JB, Wood DJ, Piasecki A, Kidder S, Ducea MN, Farley KA (2012) Late Cretaceous gravitational collapse of the southern Sierra Nevada batholith, California. Geosphere 8:314–341

Clauer N, Chaudhuri S (1996) Inter-basinal comparison of the diagenetic evolution of illite/smectite minerals in buried shales on the basis of K–Ar systematics. Clays Clay Mineral 44:818–824

Clauer N, Środon J, Francu J, Šucha V (1997) K–Ar dating of illite fundamental particles separated from illite-smectite. Clay Mineral 32:181–196

Cosca M, Stunitz H, Bourgeix A-L, Lee JP (2011) $^{40}Ar^*$ loss in experimentally deformed muscovite and biotite with implications for $^{40}Ar/^{39}Ar$ geochronology of naturally deformed rocks. Geochim Cosmochim Acta 75:7759–7778

Dallmeyer RD, Takasu A (1992) $^{40}Ar/^{39}Ar$ ages of detrital muscovite and whole-rock slate/phyllite, Narragansett Basin, RI-MA, USA: Implications for rejuvenation during very low-grade metamorphism. Contribut Mineral Petrol 110:515–527

Dodson MH (1973) Closure temperature in cooling geochronological and petrological systems. Contribut Mineral Petrol 40:259–274

Dong H, Hall CM, Peacor DR, Halliday AN (1995) Mechanisms of argon retention in clays revealed by laser $^{40}Ar$-$^{39}Ar$ dating. Science 267:355–359

Dong H, Hall CM, Halliday AN, Peacor DR, Merriman RJ, Roberts B (1997) $^{40}Ar/^{39}Ar$ of Late Caledonian (Acadian) metamorphism and cooling of K-bentonites and slates from the Welsh Basin, UK. Earth Planet Sci Lett 150:337–351

Dong H, Hall CM, Peacor DR, Halliday AN, Pevear DR (2000) Thermal $^{40}Ar/^{39}Ar$ separation of diagenetic from detrital illitic clays in Gulf Coast shales. Earth Planet Sci Lett 175:309–325

Duvall AR, Clark MK, van der Pluijm BA, Li C (2011) Direct dating of Eocene reverse faulting in northeastern Tibet using Ar-dating of fault clays and low-temperature thermochronometry. Earth Planet Sci Lett 304:520–526

Eberl DE, Środoń J (1988) Ostwald ripening and interparticle-diffraction effects for illite crystals. Am Mineral 73:1335–1345

Eberl DE, Środoń J, Kralik M, Taylor BE, Peterman ZE (1990) Ostwald ripening of clays and metamorphic minerals. Science 248:474–477

Egawa K, Lee YI (2011) K–Ar dating of illites for time constraint on tectonic burial metamorphism of the Jurassic Nampo Group (West Korea). Geosci J 15:131–135

Farley KA, Wolf RA, Silver LT (1996) The effects of long alpha-stopping distances on (U–Th)/He ages. Geochim Cosmochim Acta 60:4223–4229

Friedmann SJ, Davis GA, Fowler TK (1996) Geometry, paleodrainage, and geologic rates from the Miocene Shadow Valley supradetachment basin, eastern Mojave Desert, California. In: Beratan KK (ed), Reconstructing the history of Basin and Range extension using sedimentology and stratigraphy, Geological Society of America Special Paper 303, pp 85–105

Gehrels GE, Dickinson WR, Ross GM, Stewart JH, Howell DG (1995) Detrital zircon reference for Cambrian to Triassic miogeoclinal strata of western North America. Geology 23:831–834

Gehrels GE, Blakey R, Karlstrom KE, Timmons JM, Dickinson B, Pecha M (2011) Detrital zircon U–Pb geochronology of Paleozoic strata in the Grand Canyon, Arizona. Lithosphere. doi: 10.1130/L121.1

Gleadow AJW, Duddy IR, Green PF, Hegarty KA (1986) Fission track lengths in the apatite annealing zone and the interpretation of mixed ages. Earth Planet Sci Lett 78:245–254

Grathoff GH, Moore DM (1996) Illite polytype quantification using WILDFIRE calculated X-ray diffraction patterns. Clays Clay Mineral 44:835–842

Grathoff GH, Moore DM, Hay RL, Wemmer K (2001) Origin of illite in the lower Paleozoic of the Illinois basin: evidence for brine migrations. Geol Soc Am Bull 113:1092–1104

Haines SH, van der Pluijm BA (2010) Dating the detachment fault system of the Ruby Mountains, Nevada: significance for the kinematics of low-angle normal faults, vol 29, doi: 10.1029/2009TC002552

Hall CM, Higueras PL, Kesler SE, Lunar R, Dong H, Halliday AN (1997) Dating of alteration episodes related to mercury mineralization in the Almadén district, Spain. Earth Planet Sci Lett 148:287–298

Hall CM, Kesler SE, Simon G, Fortuna J (2000) Overlapping Cretaceous and Eocene alteration, Twin Creeks Carlin-type deposit, Nevada. Econ Geol 95:1739–1752

Halliday AN (1978) $^{40}Ar$-$^{39}Ar$ stepheating studies of clay concentrates from Irish orebodies. Geochim Cosmochim Acta 42:1851–1858

Hames WE, Bowring SA (1994) An empirical evaluation of the argon diffusion geometry in muscovite. Earth Planet Sci Lett 124:161–167

Hames WE, Cheney JT (1997) On the loss of 40Ar* from muscovite during polymetamorphism. Geochim Cosmochim Acta 61:3863–3872

Harrison TM, Grove M, Lovera OM, Zeitler PK (2005) Continuous thermal histories from inversion of closure profiles. Rev Mineral Geochem 58:389–409

Harrison TM, Célérier J, Aikman AB, Hermann J, Heizler MT (2009) Diffusion of $^{40}Ar$ in muscovite. Geochim Cosmochim Acta 73:1039–1051

Hnat JS (2009) Kinematic and temporal evolution of the southern Appalachian foreland fold-thrust belt: Constraints from structural, magnetic and radiometric analyses (Ph.D. thesis): Ann Arbor, University of Michigan, p 286

Hoisch TD (2000) Conditions of metamorphism in lower plate rocks at Bare Mountain Nevada–implications for extensional faulting, In: Whitney JW, Keefer WR (eds), Geological and geophysical characterization studies of Yucca Mountain, Nevada, A potential high-level radioactive-waste repository: U.S. Geological Survey Digital Data Series 058, CD-ROM Chapter B

Hoisch TD, Heizler MT, Zartman RE (1997) Timing of detachment faulting in the Bullfrog Hills and Bare Mountain area, southwest Nevada: inferences from $^{40}Ar/^{39}Ar$, K–Ar, U–Pb, and fission-track thermochronology. J Geophys Res 102:2815–2833

House MA, Farley KA, Kohn BP (1999) An empirical test of helium diffusion in apatite, Borehole data from the Otway basin, Australia. Earth Planet Sci Lett 170:463–474

Hower J, Hurley PM, Pinson WH, Fairbairn HW (1963) The dependence of K–Ar age on the mineralogy of various particle size ranges in a shale. Geochim Cosmochim Acta 27:405–410

Hunziker JC, Frey M, Clauer N, Dallmeyer RD, Friedrichsen H, Flehmig W, Hochstrasser K, Roggwiler P, Schwander H (1986) The evolution of illite to muscovite, mineralogical and isotopic data from the Glarus Alps, Switzerland. Contribut Mineral Petrol 92:157–180

Hurley PM, Hunt JM, Pinson WH, Fairbain HW (1963) K–Ar age values on the clay fractions in dated shales. Geochim Cosmochim Acta 27:279–284

Inoue A, Velde B, Meuner A, Touchard G (1988) Mechanism of illite formation during smectite-to-illite conversion in a hydrothermal system. Am Mineral 73:1325–1334

Jaboyedoff M, Cosca MA (1999) Dating incipient metamorphism using $^{40}Ar/^{39}Ar$ geochronology and XRD modeling: a case study from the Swiss Alps. Contribut Mineral Petrol 135:93–113

Ji J, Browne PRL (2000) Relationship between illite crystallinity and temperature in active geothermal systems of New Zealand. Clays Clay Mineral 48:139–144

Jiang W-T, Peacor DR, Árkai P, Tóth M, Kim JW (1997) TEM and XRD determination of crystallite size and lattice strain as a function of illite crystallinity in pelitic rocks. J Metamorph Geol 15:267–281

Kapusta Y, Steinitz G, Akkerman A, Sandler A, Kotlarsky P, Nagler A (1997) Monitoring the deficit of $^{39}Ar$ in irradiated clay fractions and glauconites, Modeling and analytical procedure. Geochimica et Cosmochimica Acta 61:4671–4678

Kim J-W, Peacor DR (2002) Crystal-size distributions of clays during episodic diagenesis: the Salton Sea geothermal system. Clays Clay Mineral 50:371–380

Kingsbury JA, Miller CF, Wooden JL, Harrison TM (1993) Monazite paragenesis and U–Pb systematics in rocks of the eastern Mojave Desert, California, USA: implications for thermochronometry. Chem Geol 110:147–167

Kirschner DL, Cosca MA, Masson H, Hunziker JC (1996) Staircase $^{40}Ar/^{39}Ar$ spectra of fine-grained white mica: timing and duration of deformation and empirical constraints on argon diffusion. Geology 24:747–750

Kramar N, Cosca MA, Hunziker JC (2001) Heterogeneous $^{40}Ar^*$ distributions in naturally deformed muscovite: in situ UV-laser ablation evidence for microstructurally controlled intragrain diffusion: Earth Planet Sci 192: 377–388

Kübler B (1967) La cristallinité de l'illite et les zones tout á fait supérieures du métamorphisme, *in* Etages Tectoniques, Colloque de Neuchâtel 1966, Université Neuchâtel, à la Baconnière. Neuchâtel, Switzerland

Kübler B, Jaboyedoff M (2000) Illite crystallinity. Comptes Rendus de l'Académie des Sciences 331:75–89

Lee JH, Ahn JO, Peacor DR (1985) Textures in layered silicates. Progressive changes through diagenesis and low-temperature metamorphism: Journal of Sedimentary Petrology 55:532–540

Livi KJT, Veblen DR, Ferry JM, Frey M (1997) Evolution of 2:1 layered silicates in low-grade metamorphosed Liassic shales of Central Switzerland. J Metamorph Geol 15:323–344

Markley MJ, Teyssier C, Cosca M (2002) The relation between grain size and $^{40}Ar/^{39}Ar$ date for Alpine white mica from the Siviez-Mischabel Nappe, Switzerland. J Struct Geol 24:1937–1955

McDougall I, Harrison TM (1999) Geochronology and thermochronology by the $^{40}Ar/^{39}Ar$ method, 2nd edn. Oxford University Press, New York, p 269

Merriman RJ, Frey M (1999) Pattern of very low-grade metamorphism in metapelitic rocks. In: Frey M, Robinson D (eds) Low-grade metamorphism. Blackwell Science, Oxford, pp 61–107

Merriman RJ, Peacor DR (1999) Very low-grade metapelites: mineralogy, microfabrics and measuring reaction progress. In: Frey M, Robinson D (eds) Low-grade metamorphism. Blackwell Science, Oxford, pp 10–60

Merriman RJ, Roberts B, Peacor DR (1990) A transmission electron microscope study of white mica crystallite size distribution in a mudstone to slate transitional sequence, North Wales, UK. Contribut Mineral Petrol 106:27–40

Middleton LT, Elliott DK, Morales M (2003) Tonto Group. In: Beus SS, Morales M (eds) Grand canyon geology. Oxford University Press, New York, pp 163–179

Moore DM, Reynolds RC (1997) X-ray diffraction and the identification and analysis of clay minerals, 2nd edn. Oxford University Press, New York, p 378

Mulch A, Cosca MA (2004) Recrystallization or cooling ages: in situ UV-laser $^{40}Ar/^{39}Ar$ geochronology of muscovite in mylonitic rocks. J Geol Soc 161:573–582

Mulch A, Cosca MA, Handy MR (2002) In situ UV-laser $^{40}Ar/^{39}Ar$ geochronology of a micaceous mylonite: an example of defect-enhanced argon loss. Contribut Mineral Petrol 142:738–752

Onstott TC, Mueller C, Vrolijk PJ, Pevear DR (1997) Laser $^{40}Ar/^{39}Ar$ microprobe analysis of fine-grained illite. Geochim Cosmochim Acta 61:3851–3861

Ostwald W (1900) Über die vermeintliche Isomerie des rotten und gelben Quecksilberoxyds und die Oberflächenspannung fester Körper. Zeitschrift für Physikalische Chemie, Stöchiometrie und Verwandschaftslehre 34:495–503

Parry WT, Bunds MP, Bruhn RL, Hall CM, Murphy JM (2001) Mineralogy, $^{40}Ar/^{39}Ar$ dating and apatite fission track dating of rocks along the Castle Mountain fault, Alaska. Tectonophysics 337:149–172

Perry EA (1974) Diagenesis and the K–Ar dating of shales and clay minerals. Geol Soc Am Bull 85:827–830

Petschick R, Kuhn G, Gingele F (1996) Clay mineral distribution in surface sediments of the South Atlantic: sources, transport, and relation to oceanography. Marine Geol 130:203–229

Pevear DR (1992) Illite age analysis, a new tool for basin thermal history analysis, In: Kharaka YK, Maest AS (eds), In: Proceedings of the 7th international symposium on water- rock interaction, pp 1251–1254

Rahl JM, Haines SH, van der Pluijm BA (2011) Links between orogenic wedge deformation and erosional exhumation: evidence from illite age analysis of fault rock and detrital thermochronology of syn-tectonic conglomerates ion the Spanish Pyrenees. Earth Planet Sci Lett 307:180–190

Ramírez-Sánchez E, Deckhart K, Hervé F (2008) Significance of $^{40}Ar$-$^{39}Ar$ encapsulation ages of metapelites from late Paleozoic metamorphic complexes of Aysén, Chile. Geol Mag 145:389–396

Reiners PW (2005) Zircon (U-Th)/He Thermochronometry: Rev Mineral Geochem 58:151–179

Reiners PW, Brady R, Farley KA, Fryxell JE, Wernicke B, Lux D (2000) Helium and argon thermochronometry of the Gold Butte block, south Virgin Mountains, Nevada. Earth Planet Sci Lett 178:315–326

Reuter A (1987) Implications of K–Ar ages of whole-rock and grain-size fractions of metapelites and intercalated metatuffs within an anchizonal terrane. Contribut Mineral Petrol 97:105–115

Samson SD, Alexander EC (1987) Calibration of the interlaboratory $^{40}Ar$-$^{39}Ar$ dating standard, MMhb-1. Chem Geol 66:27–34. doi: 10.1016/0168-9622(87)90025-X

Sherlock SC, Kelley SP, Zalasiewicz JA, Schrofield DI, Evans JA, Merriman RJ, Kemp SJ (2003) Precise dating of low-temperature deformation: strain-fringe analysis by $^{40}Ar$-$^{39}Ar$ laser microprobe. Geology 31:219–222

Snow JK (1992) Large-magnitude Permian shortening and continental-margin tectonics in the southern Cordillera. Geol Soc Am Bull 104:80–105

Środoń J (1999) Extracting K–Ar ages from shales: a theoretical test. Clay Mineral 34:375–378

Stevens CH, Stone P (2005a) Interpretation of the Last Chance thrust, Death Valley region, California, as an Early Permian décollement in a previously undeformed shale basin. Earth Sci Rev 73:79–101

Stevens CH, Stone P (2005b) Structure and regional significance of the Late Permian(?) Sierra Nevada-Death Valley thrust system, east-central California. Earth Sci Rev 73:103–113

Stewart JH, Gehrels GE, Barth AP, Link PK, Christie-Blick N, Wrucke CT (2001) Detrital zircon provenance of Mesoproterozoic to Cambrian arenites in the western United States and northwestern Mexico. Geol Soc Am Bull 113:1343–1356

Stockli DF, Farley KA, Dumitru TA (2000) Calibration of the apatite (U-Th)/He thermochronometer on an exhumed fault block, White Mountains, California. Geology 28:983–986

Stone P, Stevens CH (1988) Pennsylvanian and Early Permian paleogeography of east- central California: implications for the shape of the continental margin and the timing of continental truncation. Geology 16:330–333

Tagami T, Dumitru TA (1996) Provenance and thermal history of the Franciscan accretionary complex: Constraints from zircon fission track thermochronology. J Geophys Res 101:11353–11364

Turner G, Cadogan P (1974) Possible effects of $^{39}$Ar recoil in $^{40}$Ar-$^{39}$Ar dating: In: Proceedings of the 5th annual lunar and planetary science conference, pp 1601–1615

van der Pluijm BA, Lee JH, Peacor DR (1988) Analytical electron microscopy and the problem of potassium diffusion. Clays Clay Mineral 36:498–504

van der Pluijm BA, Hall CM, Vrolijk P, Pevear DR, Covey M (2001) The dating of shallow faults in the Earth's crust. Nature 412:172–174

Velde B, Renac C (1996) Smectite to illite conversion and K–Ar ages. Clay Mineral 31:25–32

Verdel C, Niemi N, van der Pluijm BA (2011a) Thermochronology of the Salt Spring fault. Constraints on the evolution of the South Virgin-White Hills detachment system, Nevada and Arizona, USA: Geosphere 7:774–784

Verdel C, Niemi N, van der Pluijm BA (2011b) Variations in the illite-muscovite transition related to metamorphic conditions and detrital muscovite content: insight from the Paleozoic passive margin of the S.W. US. J Geol 119:419–437

Warr LN, Nieto F (1998) Crystallite thickness and defect density of phyllosilicates in low- temperature metamorphic pelites: a TEM and XRD study of clay-mineral crystallinity-index standards. Candian Mineral 36:1453–1474

Warr LN, Rice AHN (1994) Interlaboratory standardization and calibration of clay mineral crystallinity and crystallite size data. J Metamorph Geol 12:141–152

Wasserburg GJ, Lanphere MA (1965) Age determinations in the Precambrian of Arizona and Nevada. Geol Soc Am Bull 76:735–758

Weaver CE (1989) Clays, muds, and shales, Developments in Sedimentology 44. Elsevier, New York, p 819

Wells ML, Hoisch TD (2008) The role of mantle delamination in widespread Late Cretaceous extension and magmatism in the Cordilleran orogen, western United States. Geol Soc Am Bull 120:515–530

Wells ML, Spell TL, Hoisch TD, Arriola T, Zanetti KA (2008) Laser-probe $^{40}$Ar/$^{39}$Ar dating of strain fringes: mid-Cretaceous syn-convergent orogen-parallel extension in the interior of the Sevier orogen: Tectonics, vol 27, TC3012, doi:10.1029/2007TC002153

Wernicke B, Axen GJ, Snow JK (1988) Basin and Range extensional tectonics at the latitude of Las Vegas. Geol Soc Am Bull 100:1738–1757

Wilkinson M, Haszeldine RS (2002) Problems with argon: K–Ar ages in Gulf Coast shales. Chem Geol 191:277–283

Wolfe MR, Stockli DF (2010) Zircon (U–Th)/He thermochronometry in the KTB drill hole, Germany, and its implications for bulk He diffusion kinetics in zircon. Earth Planet Sci Lett 295:69–82

Wright LA, Troxel BW, Burchfiel BC, Chapman R, Labotka T (1981) Geologic cross section from the Sierra Nevada to the Las Vegas Valley, eastern California to southern Nevada: Geological Society of America Map and Chart Series MC-28M

Wyld SJ, Rogers JW, Copeland P (2003) Metamorphic evolution of the Luning-Fencemaker fold-thrust belt, Nevada: Illite crystallinity, metamorphic petrology, and $^{40}$Ar/$^{39}$Ar geochronology. J Geol 111:17–38

Ziegler JF, Biersack JP, Littmark U (1985) The stopping and range of ions in solids. Pergamon Press, New York

Zwingmann H, Han R, Ree J-H (2011) Cretaceous reactivation of the Deokpori Thrust, Taebaeksan Basin, South Korea, constrained by K–Ar dating of clayey fault gouge. Tectonics TC5015. doi: 10.1029/2010TC002829